van der Hout, C.M.; Witbaard, R.; Bergman, M.J.N.; Duineveld, G.C.A.; Rozemeijer, M.J.C.; & Gerkema, T. (2017). The dynamics of suspended particulate matter (SPM) and chlorophyll- a from intratidal to annual time scales in a coastal turbidity maximum. *Journal of Sea Research*, 127, 105-118

Published version: https://dx.doi.org/10.1016/j.seares.2017.04.011

Link NIOZ Repository: www.vliz.be/nl/imis?module=ref&refid=289483

The dynamics of suspended particulate matter (SPM) and chlorophyll-a from intratidal to annual time scales in a coastal turbidity maximum

C.M. van der Hout[1]
R. Witbaard[1]
M.J.N. Bergman[2]
G.C.A. Duineveld[2]
M.J.C. Rozemeijer[3]
T. Gerkema[1]

[1]NIOZ Royal Netherlands Institute for Sea Research, Department of Estuarine and Delta Systems (EDS), and Utrecht University, P.O. Box 140, 4400 AC Yerseke, The Netherlands
[2]NIOZ Royal Netherlands Institute for Sea Research, Department of Ocean Systems (OCS), and Utrecht University, P.O. Box 59, 1790 AB Den Burg, The Netherlands
[3]IMARES Wageningen UR, P.O. Box 68, 1970 AB IJmuiden, The Netherlands

E-mail corresponding author: carola.van.der.hout@nioz.nl

Abstract

The analysis of 1.8 years of data gives an understanding of the response to varying forcing of suspended particulate matter (SPM) and chlorophyll-a (CHL-a) in a coastal turbidity maximum zone (TMZ). Both temporal and vertical concentration variations in the near-bed layer (0 – 2 m) in the shallow (11 m deep) coastal zone at 1 km off the Dutch coast are shown. Temporal variations in the concentration of both parameters are found on tidal and seasonal scales, and a marked response to episodic events (e.g. storms). The seasonal cycle in the near-bed CHL-a concentration is determined by the spring bloom. The role of the wave climate as the primary forcing in the SPM seasonal cycle is discussed. The tidal current provides a background signal, generated predominantly by local resuspension and settling and a minor role is for advection in the cross-shore and the alongshore direction. We tested the logarithmic Rouse profile to the vertical profiles of both the SPM and the CHL-a data, with respectively 84% and only 2% success. The resulting large percentage of low Rouse numbers for the SPM profiles suggest a mixed suspension is dominant in the TMZ, *ie*. surface SPM concentrations are in the same order of magnitude as near-bed concentrations.

Keywords

Wave climate // In-situ observations // Bed shear stress // SPM // chlorophyll-a // season

Highlights

- The seasonal SPM variation is primarily driven by the seasonal wave climate
- SPM and CHL-a concentrations have an opposed seasonal cycle
- The tidal current generates a background signal in both concentrations
- The majority of SPM profiles fit to the Rouse profile

1. Introduction

Coastal areas all over the world are under constant pressure due to the growth of the world population and climate change. Currently implemented coastal adaptations to counteract the effects of climate change may affect the local ecology and the surrounding ecosystem. In the Netherlands, several engineering solutions have been developed and implemented to mitigate negative effects on the ecosystem (Borsje et al., 2011; De Jong et al., 2015). Understanding the effect of these solutions on the ecosystem requires basic knowledge of the coastal system in both the physical and the ecological sense. One parameter to consider in the Dutch coastal zone is suspended particulate matter (SPM), as the coastal zone forms a transport route of SPM from the Strait of Dover and rivers towards the Wadden Sea. SPM is composed of organic and terrigenous particles and its concentration and variation affects the pelagic as well as the benthic ecosystem.

In the southern North Sea, highest SPM concentrations are found close to the coasts as observed by many surface observations such as remote sensing data (Eleveld et al., 2008; Fettweis et al., 2007; Van Raaphorst et al., 1998), and *in-situ* data (Dyer and Moffatt, 1998; Fettweis et al., 2007; Howarth et al., 2002; Huthnance, 1997; Van Alphen, 1990; Visser et al., 1991). More specifically for the Dutch coast, a near-bed turbidity maximum zone (TMZ) is present along the coastline at a maximum distance of 3 km from the shore (Van Alphen, 1990; Van der Hout et al., 2015). Thus high SPM concentrations are close to the coast and nearby engineering solutions. All along the coastline SPM is accumulating in cross-shore direction in the TMZ (Visser et al., 1991) and is transported northwards (Van der Giessen et al., 1990) forming a “coastal river of silt”. The majority of the northward transport of SPM along the coast, and also of nutrients, plankton, fish larvae and other juvenile marine fauna, may be concentrated in this small region. The TMZ is likely to control the distribution of macrobenthos, and the prey items of higher trophic levels such as predatory fish or birds (Van der Veer et al., 2015), by its high turbidity and nutrient levels. It is in this same zone that high densities of the benthic bivalve *Ensis directus* have been observed (Witbaard et al., 2015), which is a filter feeder thriving on suspended (phytoplankton) particles. These bivalves may contribute to the accumulation of SPM in the TMZ by (seasonal) burial of SPM into the seabed (Witbaard et al., 2016; this volume).

Processes that affect the levels of SPM concentrations in the southern North Sea are depth, tidal currents, biota, waves and density driven currents (Fettweis et al., 2014; Stanev et al., 2009; Visser et al., 1991). The tidal wave in this area propagates in an anti-clockwise direction and generates strong tidal currents near the coasts. In combination with waves, high bed shear stresses are generated (Stanev et al., 2009) and fine bottom particles are resuspended. Unraveling the response of SPM and CHL-a concentrations to the tidal regime, the waves or biological factors has been subject of many field studies. Variations in SPM and CHL-a linked to tidal regimes were reported by Bass et al. (2002), Blauw et al. (2012), Joordens et al. (2001), McCandliss et al. (2002) and Orton and Kineke (2001). Studies in Liverpool Bay and Jiaozhou Bay highlighted a wave-related dependence of the SPM concentration (Fettweis et al., 2012; Krivtsov et al., 2012 and references therein). SPM concentrations in the Dutch and Belgian coastal zone are higher in winter than in summer, which has been linked to the seasonal pattern in storms (Eleveld et al., 2008; Fettweis et al., 2012; Visser et al., 1991). However, in recent research in the Belgian coastal zone (bordering the Dutch coast) this seasonal pattern is hypothesized to be related to the seasonal cycle in the phytoplankton population (Fettweis et al., 2014). The phytoplankton population is determined by light, nutrient availability, temperature and grazing, and on the other hand the population affects flocculation of SPM (Jago et al., 2007; Jones et al., 1998; Passow, 2002) and hence acts as a seasonal biological process affecting the fall velocity of SPM.

The focus of this study is to describe the processes that control the temporal variation of SPM and CHL-a concentrations in the near-bed water layer (0 – 2 m) in the TMZ along the Dutch coast. The seasonal cycle is our main interest, but also smaller scales down to the tidal cycle will be analyzed. The dataset for the analysis was obtained with an instrumented bottom frame deployed in the TMZ for a period of almost 2 years. Details of the instrumentation and the specifics of the location of bottom frame are given in Section 2, as well as details on the methods applied to analyze the dataset. The time-series includes storm conditions, periods for which data is otherwise difficult to obtain due to unworkable high swell or clouds obscuring satellite imagery. The effects of the wave climate and the tide on the instant concentrations and on the seasonal cycle is presented in Section 3. Additionally, we will discuss the suspension mode over time on basis of the Rouse number, R_n. The validity of the Rouse profile will first be discussed in section 3.3, as several of the assumptions for the equilibrium profile are violated in the research area (Mehta, 2014; Orton and Kineke, 2001). If valid, the near-bed measured concentrations can be extended up to the surface with the logarithmic Rouse number (Mehta, 2014). We will use the Rouse number to estimate the suspension mode; either a near-bed dominated suspension (high R_n) or a mixed suspension (low R_n) in which the SPM is more uniformly distributed over the water column (Mehta, 2014). In Section 4 we will discuss the (interaction of the) seasonal cycles of the SPM and CHL-a concentrations, the resuspension and advective character of the tidal oscillation and the effect of the suspension mode for transport estimations. In Section 5 we conclude with a description of the character of the SPM suspension near the seabed in the coastal TMZ in which the tide and the wave climate each play a role.

2. Methods

2.1. Location and field observations

2.1.1. Bottom frame location

The study area is located along the Dutch coast, 20 km north of the harbor of IJmuiden, in the southern North Sea (Figure 1). In 2011 and 2012, a bottom frame was deployed 1.2 km offshore (52°38.249’N; 4°36.294’E) for the project ‘Monitoring and Evaluation Program Sand mining’ commissioned by the La Mer Foundation (Witbaard et al., 2015). The average water depth was 11 m. The bottom frame was located 0.6 km south of the Egmond transect, which was surveyed in 2003, 2010 and 2011 to study the location of the turbidity maximum zone (TMZ) along the coast (Van der Hout et al., 2015). The bottom frame was deployed in this TMZ, landward of the average position of the observed peak concentration. One of the measured transects is depicted in Figure 1B to illustrate the spatial context. The study area is located 80 km north of the Rhine outflow in the far-field plume of the region of freshwater influence (ROFI) (Simpson et al., 1993).Temporary vertical stratification has been observed at the study site (Rijnsburger et al., 2016; Van der Hout et al., 2015) as well as at a location 5 km further offshore (Nauw and Van der Vegt, 2012). The seabed at the study site is sandy with a median grain size of 222 µm, the d_{50} is 181 µm (fine sands), with a clay percentage of 5% in the top layer of 0.05 m (Witbaard et al., 2016; this volume).

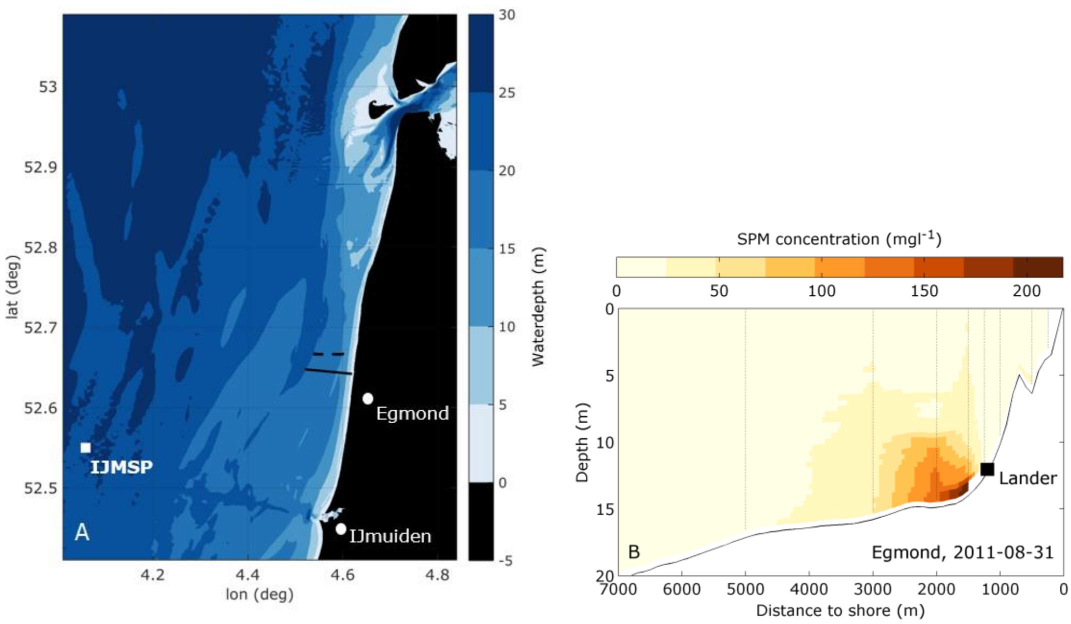

Figure 1. A. Map of the research area (Rijkswaterstaat), with the location of the bottom frame (black square) and the two Egmond transects in black lines (dashed: 2003, straight: 2010-2011) near Egmond. The KNMI wind station is in IJmuiden and the Rijkswaterstaat wave buoy IJMSP is indicated by a white square. B. The location of the bottom frame is indicated with reference to a cross-sectional

profile of the SPM concentration along the Egmond transect (August 31, 2011), based on a sequence of vertical profiles at the vertical dashed lines (Van der Hout et al., 2015).

2.1.2 Wind and wave climate

The wind climate at the Dutch coast is characterized by a dominance of southwesterly winds, plus a smaller peak for northerly winds (Figure 2). Both observational years 2011 and 2012 show a stronger dominance of southwesterly winds than in the 10-year average. The wind climate produces a seasonal pattern in the wave climate with a higher wave height and variance in autumn and winter, and lower wave height and variance in spring and summer (Figure 3A).

The wave data used in this study are from the wave buoy Munitiestortplaats IJmuiden (IJMSP; Figure 1A). Waves are categorized into storm conditions (H_s > 3.5 m, 5% of time), intermediate conditions (H_s = 2 – 3.5 m, 27% of time) and calm conditions (H_s < 2 m, 68% of time). Storm waves are mostly formed by the northwesterly winds (Figure 3B) due to the largest fetch length in the North Sea. Calm waves have a median westerly direction (thus coming equally from the north and south), except for spring when the median direction is NW. The intermediate category waves approach the coast mostly from southerly direction. The wave buoy (35 km offshore) also measured waves from an easterly direction. These wave records are neglected in the analysis, as at 1.5 km from the shore (our study area) such waves have barely developed.

Compared to the 10-year average, spring 2011 had milder wave conditions (Figure 3B). In September 2011 ex-hurricane Katia caused wind speeds > 9 Bft and H_s > 4 m followed by an extremely calm November, and an extremely turbulent December with an average wave height in the intermediate category. Winter 2011-2012 had twice as many storms as normal with four cyclone passings over the North Sea (Roberts et al., 2014), followed by milder wave conditions than normal in February and March 2012.

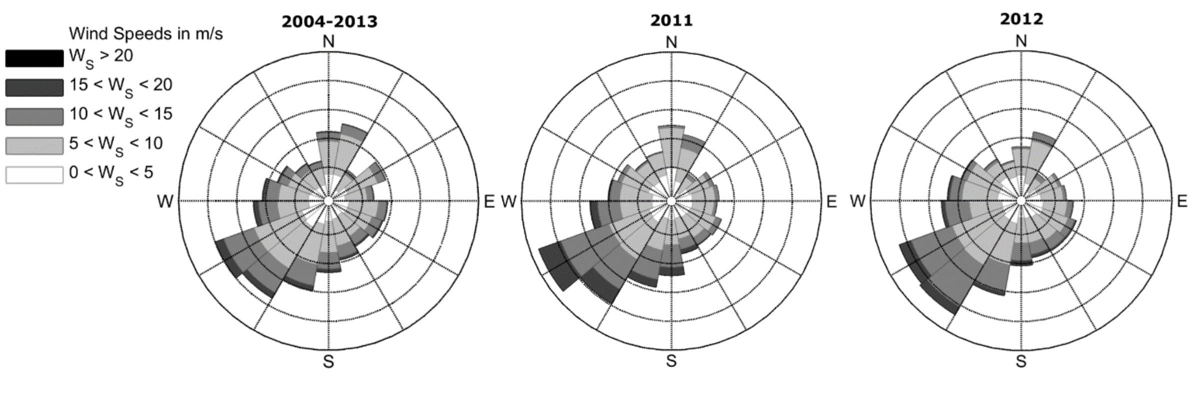

Figure 2. Wind roses for the 10-year average (left) and for the years 2011 and 2012. The radial scale of the frequency is 1.4%. Data are provided by KNMI, for location IJmuiden and based on the hourly average.

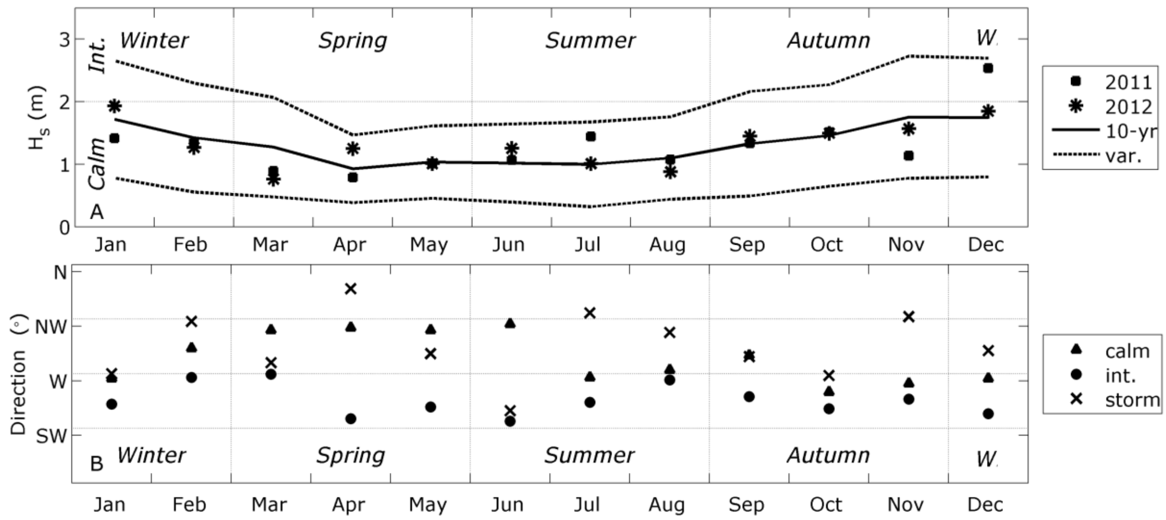

Figure 3. Seasonal variation of the wave climate (Data from Rijkswaterstaat). A. The 10-year (2004-2013) monthly average and variance of the significant wave height (H_s; calm and intermediate (int.) categories indicated) and the monthly average for 2011 and 2012 (upper panel). B. The monthly median wave direction per wave height category; calm (H_s < 2 m), intermediate (int.; H_s = 2 – 3.5 m) and storm (H_s > 3.5 m) of 10-years of data.

2.1.3. Instrumentation

The bottom frame consisted of a triangular aluminum construction with sides of 2 m long and 2 m high (Witbaard et al., 2015). The frame was equipped with a series of sensors to measure current velocity, turbulence, water depth, temperature, salinity, turbidity and fluorescence. All data was gathered at an interval of 10 minutes. A Nortek Vektor ADV was mounted on the frame at a height of 0.3 mab, with the measurement cell at 0.15 mab. The instrument was set to record a burst interval of 2 minutes at 1 Hz every 10 minutes. Temperature and salinity were measured with a pumped version of the Sea-Bird SBE 37-SM MicroCAT at 1.4 mab. Turbidity and fluorescence were measured optically with ALEC-JFE Advantech Compact-CLW's at four heights above the bottom, i.e. at 0.3, 0.8, 1.4 and 2.0 mab. The sensor at 0.3 mab was the INFINITY version to measure turbidities > 2 gl^{-1}. The average of a burst of 10 measurements at 1 Hz was used in the analysis.

The deployment period ran from February 25, 2011 until November 24, 2012. The bottom frame was replaced 17 times with intervals between three to ten weeks with a duplicate frame equipped with a clean set of instruments. The duration of the individual deployment periods depended on the season. In spring and summer short periods of three weeks were necessary to limit the effects of biofouling. In autumn and winter, storms sometimes led to longer deployment periods due to operational limits. Besides the short data gaps - up to one day - related to the frame replacements, also longer gaps exist in the data of individual instruments due to loss of battery power when deployment periods became too long or because of malfunctioning of instruments, tilting of the frame or biofouling.

2.2. Data analysis

The horizontal components of the velocity are rotated with 6 degrees clockwise to align the currents with the coastline, so that v_l is the alongshore current velocity and v_c the cross-shore velocity. For some analyses an average was calculated over the tidal cycle, i.e. over the period between two successive slacks after flood.

2.2.1. Optical sensor calibration

The optical sensors have been calibrated at the start of the project with settled fine sediments which were collected during a previous mooring at the study site. Calibration concentrations ranged from 6 mgl^{-1} to 2 gl^{-1} for SPM and 0.7 – 475 µgl^{-1} for CHL-a. The calibration gave a linear response between 20 and 2000 mg l^{-1} for SPM ($R^2 > 0.95$), and between 2 and 475 µg l^{-1} for CHL-a ($R^2 > 0.95$). The used type of optical sensors is known for their stability over long time spans. However, a single calibration cannot account for variations in sediment composition throughout the year or during large resuspension events or varying phytoplankton community compositions. A different type of optical sensor applied in the study site showed a deviation in the calibration of a factor two (Van der Hout et al., 2015).

2.2.2. Grain-size distribution of SPM

At approximately 1 m above the seabed water samples were collected with Niskin bottles during the bottom frame replacement cruises. A 1 l water sample was stored at 4 ^{o}C for two days to let sediments settle, then decanted and analyzed in a Beckman Coulter Laser LS 13 320. The samples were only treated with 20 s ultrasonic sound before analysis. Ultrasonic sound may produce air bubbles in the range 100 – 600 µm (pers comm. J.B. Stuut), but these were not found in the spectra. Similarly, also a 10 l water sample was stored at 4 ^{o}C, decanted and treated in three steps to remove three types of organic components, following the procedure described in Stuut et al. (2014). The first treatment concerned the removal of organic tissue with H_2O_2. The second and third treatments with HCl and NaOH aimed to remove biogenic calcium-carbonate and biogenic silicates respectively. The remaining fraction is called the insoluble or terrigenous fraction. Visual inspection of microscope images was done to ensure complete removal of the organic particles. The samples were split into two subsamples before the treatments, one subsample for the analysis of the grain-size distribution and one subsample to determine the mass changes per treatment. For the mass analysis the subsamples were centrifuged and freeze-dried after treatment and then weighed to determine the reduction in weight.

2.2.3. Bed shear stress from ADV

For the calculation of the bed shear we followed the procedure in Verney et al. (2007) with the exception that wave shear stress was determined according to the method of Van Rijn (2007). The latter gives an all inclusive bed roughness predictor for a combination of currents and waves with all bed forms in the field. The mean bed shear stress is calculated with (Verney et al., 2007);

$$\tau_m = \tau_c \left(1 + 1.2 \left(\frac{\tau_w}{\tau_w + \tau_c}\right)^{3.2}\right) = \tau_{TKE} = 0.5\rho C \sqrt{u_t'^2 + v_t'^2 + w_t'^2} \qquad (1)$$

with $(u_t'^2, v_t'^2, w_t'^2)$ calculated from the spectral analysis of the fluctuating part of the velocity (u', v', w') (Soulsby and Humphery, 1990). The constant *C* has been found to approximate 0.19 for a wide variety of flows (Verney et al., 2007). The fluctuating velocities are first despiked with the phase-space thresholding method developed by Mori et al. (2007) and Goring and Nikora (2002). The method requires a longer time series than the burst length to separate the spikes from the standard deviation. Therefore all data is merged and the despike method is applied on subsets with a length of 250.000 data points. Subsequently the data are separated back into burst intervals. Spectra are obtained from the despiked burst intervals with the fast-fourier transform, and are averaged over an hour. In the logarithmic space of the (averaged) spectra, the separation between the turbulent velocities and the wave orbital velocities is drawn as a linear line between the (non-logarithmic) frequencies 0.04 and 0.31 Hz. This range of wave frequencies covers both swell and wind waves (bimodal wave spectrum) and is well outside the influence of the Nyquist frequency (f_N = 0.5 Hz). The two resulting surface areas of the linear spectra are $u_t'^2, v_t'^2, w_t'^2$ (turbulent variance) and $u_w'^2, v_w'^2, w_w'^2$ (wave variance). When no waves are present, the separation line follows the inertial slope of the spectrum. The 1 Hz frequency and the 120 s burst length of the measurements proved to be just high and long enough - when averaged over one hour - to distinguish the ranges of the wave orbital velocities from the inertial subrange, and thus to separate the turbulent and wave signals from each other.

An important parameter in the calculation of the wave shear stress is the bed roughness (k_s or z_0), as its value can vary within 2 orders of magnitude. The bed roughness depends on the bed form, which may alter quickly when conditions change, and is thus a sensitive parameter. After evaluating various bed roughness predictors for a similar coastal site off Terschelling (The Netherlands, water depth 5 - 10 m, sand of 200 µm, orbital velocities up to 0.6 ms^{-1}), Houwman (2000) advised a constant bed roughness (k_s) of 0.1 m. He stated that a uniform bed roughness was the optimum estimate for all flow conditions, with a similar accuracy as the uniform bed roughness predictor by Van Rijn (2007).

The wave friction factor f_w is then calculated as (Van Rijn, 2007)

$$\mathrm{f_w} = \exp\left(-6 + 5.2\left(\frac{\mathrm{U_w T_p}}{2\pi \mathrm{k_s}}\right)^{-0.19}\right) \tag{2}$$

With U_w and T_p determined from the ADV. The wave period T_p was determined from the frequency of the highest spectral peak from the pressure sensor. The representative bottom orbital velocity (U_w) is determined from the wave variance of the velocity spectrum, with (Wiberg and Sherwood (2008))

$$\mathrm{U_w} = \sqrt{2} \cdot \sqrt{\mathrm{u}_w'^2 + \mathrm{v}_w'^2} \tag{3}$$

The wave shear stress (τ_w) and the wave-current shear stress (τ_{wci}) are then obtained with (Verney et al., 2007):

$$\tau_w = 0.5\rho \mathrm{f_w} \mathrm{U_w^2} \tag{4}$$

$$\tau_{wci} = \tau_{max} = \sqrt{(\tau_m + \tau_w \cos(\Psi))^2 + (\tau_w \sin(\Psi))^2} \tag{5}$$

With Ψ the angle between the wave direction (from wave buoy) and the current direction ($\bar{u}$, $\bar{v}$).

2.2.4. Rouse number

The Rouse profile describes in a simple way the logarithmic distribution of the SPM over depth by capturing the vertical profile in one number; the Rouse number R_n. The Rouse equation is based upon the equilibrium state of the concentration, in which the vertical upward flux by turbulence and the gravitational settling are in balance (Rouse, 1950). It is assumed that gradients in the advective (i.e. horizontal) transport are much smaller than in the vertical and therefore negligible. The common representation of the Rouse equation is (Mehta, 2014)

$$\frac{C(z)}{C_a} = \left[\frac{z_a(h-z)}{z(h-z_a)}\right]^{w_s/\kappa u_*} \tag{6}$$

With the reference concentration $C_a = C(a)$ at reference height $z = z(a) = z_a$, h = water depth, w_s = settling velocity, κ = Von Karman constant and u_* = the friction velocity. The eddy diffusivity is described with a parabolic form, which assumes the absence of stratification. The settling velocity is assumed to be independent of the sediment concentration and the shear rate. The dimensionless ratio in the exponent of equation (6) is the Rouse number $R_n = w_s/\kappa u_*$ (Rouse, 1950). It represents the ratio between the downward motion of the sediment by gravity and the upward force by the turbulent motion. The value of R_n gives an indication of the suspension mode; a high R_n represents a steep concentration gradient, and a low R_n a nearly uniform profile. The separation between both modes is usually drawn at R_n = 0.8 (Mehta, 2014).

The Rouse number is calculated from an observed profile by rewriting equation (6) (Mehta, 2014):

$$R_n = \frac{-\log(C/C_a)}{-\log((z_a\,(h-z))/z(h-z_a))} \qquad (7)$$

The reference concentration C_a is taken at z_a = 0.3 mab: the observation closest to the seabed. For the calculation of R_n, the SPM and CHL-a concentrations have been smoothed with a low pass band filter with a 50 minutes window. The nominator and the denominator on the right-hand side of equation (7) were calculated for each of the 3 remaining heights z = [0.8, 1.4, 2.0] mab and with h = 11 m. R_n is the coefficient of the linear regression without offset through these three points if R^2 > 0.95. If R^2 is less than 0.95, we assume that the vertical concentration distribution does not follow a Rouse profile. R_n could not be calculated for the period between October 2011 and early January 2012 since the optical sensor at 2.0 mab malfunctioned in this period, and not enough information was available for a reliable regression.

3. Results

3.1. Hydrography

3.1.1. Local environmental conditions

The study area shows a seasonal cycle in the water temperature (Figures 4F and 5F) ranging from 3 °C in February 2012 to 20 °C in August 2012. A tidal fluctuation of maximum 1 °C is sometimes apparent during calm conditions such as in November 2011 and February 2012. The salinity is relatively low due to the large Rhine river outflow and varies between 25 and 32 PSU, generally with values close to 30 PSU (Figures 4G and 5G). Fluctuations with a magnitude of maximum 2 PSU occur on a tidal scale. There is no distinct seasonal pattern in salinity but larger fluctuations occur on time scales of weeks to months. Lowest salinities occurred in January 2012. The tidal range varied over the spring-neap cycle between 1.1 and 1.9 m (Figures 4E and 5E). The near-bed alongshore velocity amplitude ranged between 0.5 and 0.2 ms^{-1} over the spring-neap cycle. The spring-neap cycle is clearly present in the water level signal, but is distorted in the velocity signal by intermediate and storm waves.

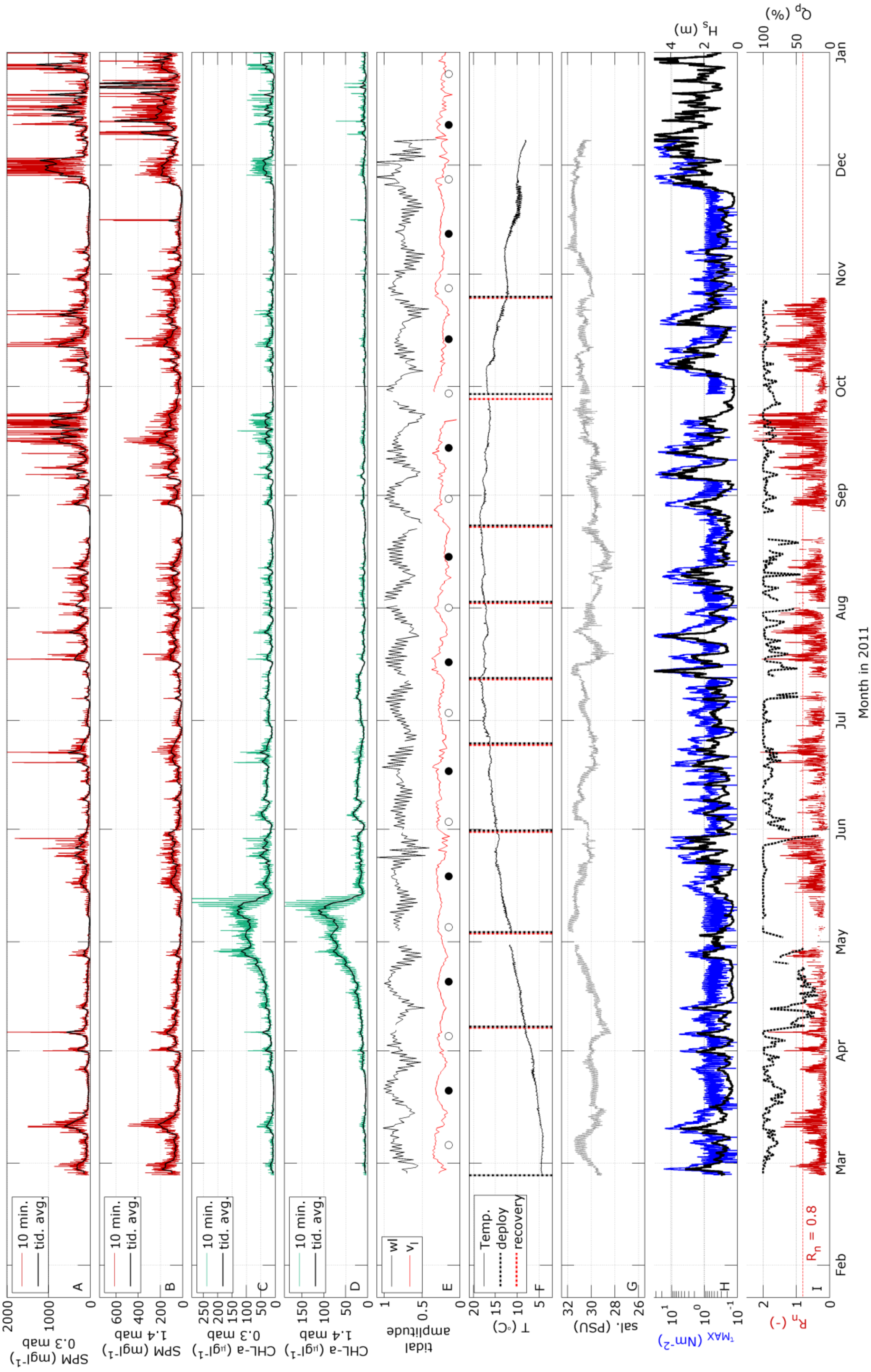
SPM (mgl-1) 0.3 mab
SPM (mgl-1) 1.4 mab
CHL-a (μgl-1) 0.3 mab
CHL-a (μgl-1) 1.4 mab
tidal amplitude
T (°C)
sal. (PSU)
τMAX (Nm-2)
Hs (m)
Rn (-)
Qp (%)
10 min.
tid. avg.
wl
vl
Temp.
deploy
recovery
Rn = 0.8
A
B
C
D
E
F
G
H
I
Feb
Mar
Apr
May
Jun
Jul
Aug
Sep
Oct
Nov
Dec
Jan
Month in 2011

Figure 4 (A-I). Data recorded at the bottom frame in 2011. SPM concentrations at the lowest observation (0.3 mab, panel A) and at 1.4 mab (panel B) including the tide-averaged value (black lines). CHL-a concentrations at the lowest observation (0.3 mab, panel C) and at 1.4 mab (panel D) and their tide-averaged value (black lines). Panel E shows the tidal amplitude of the water level and the alongshore tidal current. The moon phases (full moon; ○, and new moon; ●) are shown; spring tide is two days after full and new moon. Panel F shows the temperature signal, and the deployment and recovery dates as well. Panel G shows the salinity. Both the bed shear stress (τ_{MAX}*; blue) and the significant wave height (*H_s*; black, source; Rijkswaterstaat) are shown in panel H. The Rouse number* R_n*, and the percentage of fitted Rouse profiles per tidal cycle,* Q_p*, are shown in panel I.*

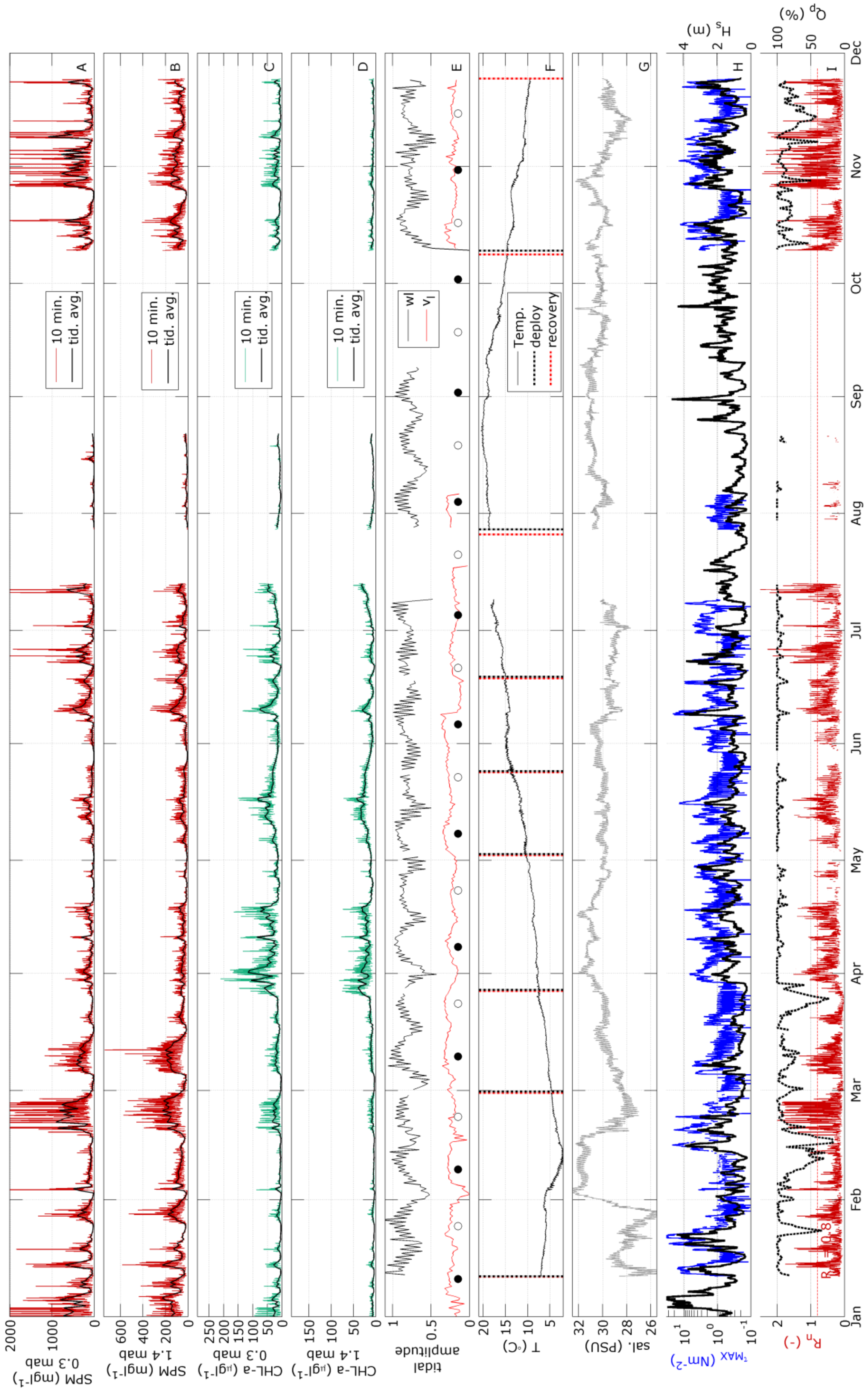
A
B
C
D
E
F
G
H
I
10 min.
tid. avg.
wl
v_l
Temp.
deploy
recovery
SPM (mgl-1) 0.3 mab
SPM (mgl-1) 1.4 mab
CHL-a (μgl-1) 0.3 mab
CHL-a (μgl-1) 1.4 mab
tidal amplitude
T (°C)
sal. (PSU)
τ_MAX (Nm-2)
H_s (m)
R_n (-)
Q_p (%)
R_n = 0.8
Jan
Feb
Mar
Apr
May
Jun
Jul
Aug
Sep
Oct
Nov
Dec
Month in 2012

Figure 5 (A-I). As in Figure 4, but for 2012.

3.1.2. Grain size suspended particles

Only five water samples contained enough SPM to measure the grain size of the terrigenous sediment fraction. The grain-size distributions (Figure 6; solid lines) of the terrigenous particles entail the clay fraction (< 2 µm) and the silt fraction (< 63 µm). Peaks in the distributions are at 0.4 µm, 5 µm, 10 µm and 30 - 50 µm, which are present regardless of the time in the year. The mode of the terrigenous particles is at 10 ± 5 µm (Figure 6, solid lines). The modes of the untreated (but sonified) samples have the same values (dashed lines in Figure 6). However, the tails of the bell-shaped distribution are different before and after treatment. All samples except of Feb 2012 have particles in the range 50 – 200 µm, which is the typical range for phytoplankton; both biogenic silicates and foraminifera (Stuut et al., 2002). Notably, the clay fraction is more present in the treated samples than in the untreated. An explanation could be that before the treatment this fraction was still captured in flocculi with a size similar to silt, despite the high turbulence in the measurement volume of the Coulter Laser (the exact value is not calculated). After chemical treatment these flocculi have disintegrated into their primary small particles, pointing at a strong aggregation of the clay particles.

The mass analysis shows that the SPM consists for 35 - 55% of organic particles, being: organic tissue (10 – 15%), biogenic silicate (0 – 20 %) and biogenic calcium-carbonates ($CaCO_3$; 25 – 30 %). A seasonal trend analysis is not possible due to the limited amount of samples (5). The high organic content in the samples suggests that at our study site the terrigenous particles are mostly present in aggregated form, as observed by others in similar environments (Fettweis et al., 2014; Jones et al., 1998).

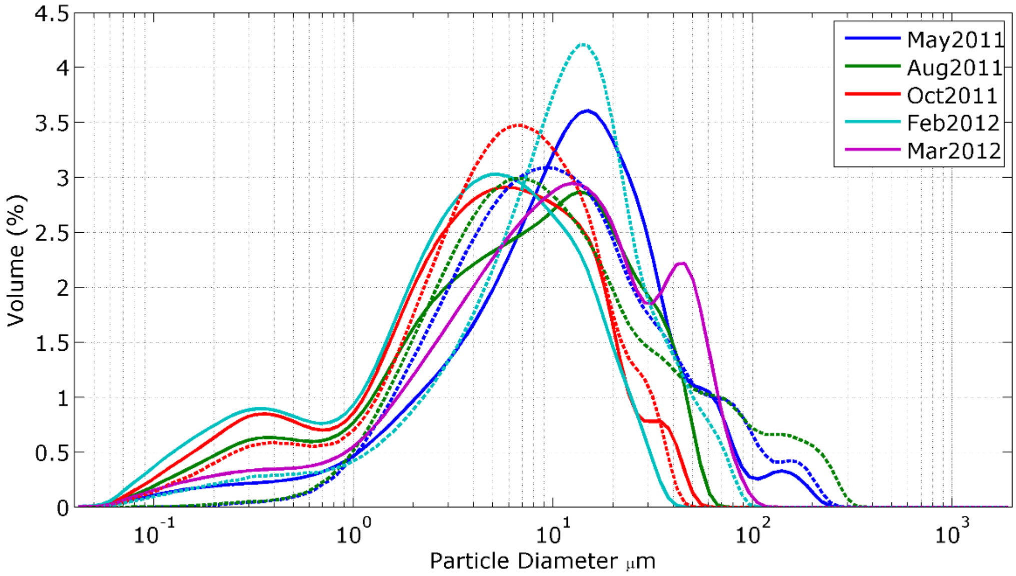

Figure 6. The grain size distribution of five samples before treatment (dashed lines) and after treatment (solid lines)

3.1.3. Bed shear stress

The bed shear stresses varied between 0.1 and 40 Nm^{-2} (Figures 4H and 5H) and has a wave and a tidal component. The bed shear stress exerted by waves is 1 - 2 orders of magnitude larger than the range due to the tidal variation which is between 0.2 and 1 Nm^{-2} during calm conditions (Figures 4H and 5H). The scatter plot in Figure 7 indicates a positive logarithmic relation between the bed shear stress and the significant wave height for H_s > 0.8 m. The variation around the median is due to the tidal variation.

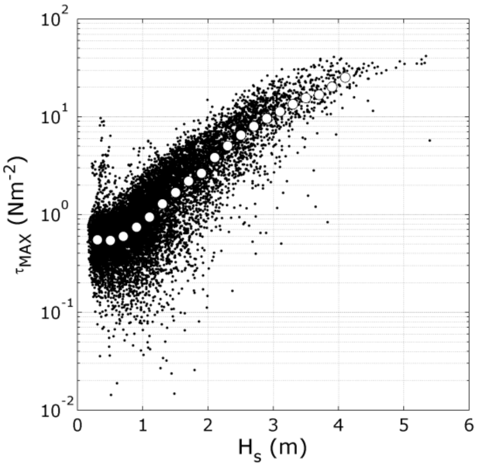

Figure 7. Scatter plot of the bed shear stress (τ_{MAX}) versus the significant wave height (H_s; 1 hr intervals). The large white dots are the median bed shear stresses per 0.2 m H_s bins.

3.2. SPM and CHL-a variation

3.2.1. SPM concentrations

Panels A and B in Figures 4 (for 2011) and 5 (for 2012) show the SPM concentrations at 0.3 mab and at 1.4 mab. The SPM concentrations ranged from lower than 20 mgl^{-1} and attained at least 2 gl^{-1} (the limits of the linear gain of the optical sensors). The time series shows fluctuations of the SPM concentration on both the short term (tidal scale, regular) and the long term (storms, irregular). The tidal SPM variation (panels A and B) increases during intermediate ($2 < H_s < 3.5$ m) and storm ($H_s > 3.5$ m) conditions and decreases afterwards during calm conditions (H_s in panels H). The peaks in the SPM concentration occur at an irregular interval and seem related to elevated bed shear stresses due to increased wave heights (both Figures 4H and 5H). At 0.3 mab the SPM concentrations in these peaks range from between 0.5 gl^{-1} to at least 2 gl^{-1}. In spring and summer, peaks barely exceed 1 gl^{-1}, while in the 2011-2012 winter all five storms caused elevated SPM concentrations exceeding 2 gl^{-1}. Even the SPM concentrations at 1.4 mab reached up to 1 gl^{-1} in December 2011, far higher than the average peaks of 0.5 gl^{-1} during the remainder of the year. January and February 2012 remained turbid with concentrations regularly exceeding 1 gl^{-1} at 0.3 mab, while spring was a calm period with relatively low peak concentrations of around 0.5 gl^{-1}. In the summer of 2012 concentrations regularly exceeded 1 gl^{-1}, and in autumn two storms ($H_s > 3.5$ m) passed during our deployments, but unfortunately the SPM concentrations were not recorded due to failing devices. Later in autumn concentrations exceeded 2 gl^{-1} a few times at 0.3 mab.

3.2.2. CHL-a concentrations

Panels C and D in Figures 4 (for 2011) and 5 (for 2012) show CHL-a concentrations between 3 μgl^{-1} to at least 300 μgl^{-1} at 0.3 mab and 1.4 mab. The concentration at 0.3 mab is always higher than at 1.4 mab. Both the relatively high concentrations (the order of surface concentrations is 10 μgl^{-1} (Joordens et al., 2001)) and the increase towards the seabed illustrate that the observed CHL-a at 0.3 mab is an accumulated suspension near the seabed. The CHL-a concentration shows variations on both the regular tidal and the irregular storm scale, similar to what was observed for the SPM concentrations and most likely related to resuspension of the accumulated suspension. The dominant variation in the CHL-a concentration is the increase in spring and decrease in summer: the spring bloom. There are differences in the development and magnitude of the spring bloom of both years. In 2011 the CHL-a concentration at 0.3 mab built up in April during calm conditions, and the near-bed peak occurred half of May with tide-average concentrations of 125 μgl^{-1} and peaks of > 300 μgl^{-1}. In 2012 the CHL-a concentration started to build up at the end of March, but stopped at the end of April. Concentrations had reached near-bed peaks of 200 μgl^{-1} and tide averaged concentrations 100 μgl^{-1}, somewhat lower than in 2011. In April 2012 several periods characterized by intermediate wave conditions occurred which seem to have suppressed the further development of the phytoplankton bloom. Figure 3A suggests that April 2012 was a period with higher wave energy input and deviates from the long term average conditions. Half of May 2012 concentrations increased again to similar tide-averaged concentrations as in April. Other, short-lived peaks in the CHL-a concentration at 0.3 mab occurred at moments of increased bed shear stresses at the same instant that SPM concentrations increased. These peaks can be up to 100 μgl^{-1}, even in winter. Tide-averaged concentrations at 1.4 mab attained 100 μgl^{-1} in spring 2011 and 40 μgl^{-1} in spring 2012, which are only slightly lower than at 0.3 mab. Conversely, the incidental wave-related peaks at 1.4 mab are an order of magnitude lower and rarely exceed 15 μgl^{-1}.

3.2.3. The seasonal scale

Figure 8 shows the GAM smoothed yearly variations of SPM and CHL-a at 0.3 mab on the basis of weekly average concentrations (Generalized Additive Model; Wood (2006)). The GAM model estimates a smoother function describing the seasonal variation for each year. The smoother functions for each variable (CHL-a, SPM) and each year were significant. This shows that there is a seasonal variation in the near-bed concentrations of both CHL-a and SPM. At the same time the smoother functions for each variable are compared for a difference between years. This comparison showed that the seasonal development of near-bed CHL-a concentrations differed between 2011 and 2012. Such a seasonal difference could not be demonstrated for the near-bed SPM concentrations. The near-bed CHL-a concentrations show a sharp peak in 2011 and a wide peak in 2012 (Figure 8A). In the summer period of 2011 the near-bed SPM concentrations show minimum values but in 2012 these minimum values are overshadowed in June (Week 26; Figure 8B) when intermediate waves hit the Dutch coast (Figure 5H).

Winter weekly-averaged SPM concentrations reach 250 mgl^{-1}, summer values are between 50 and 150 mgl^{-1}. The near-bed CHL-a increase related to the spring bloom starts in week 11 (2011) or week 6 (2012) when average concentrations increase from lower than 10 μgl^{-1} to 30 - 60 μgl^{-1} and decrease at the end of May (week 20). The autumn and winter values remain elevated around 10 μgl^{-1} and show oscillations with the wave climate. The spring bloom related CLH-a increase in 2012 seems to start in February (Figure 8A), but from the raw time-series in Figure 6C it follows that the CHL-a increased temporarily in February and March due to two intermediate wave events, and the steep increase started at the end of March.

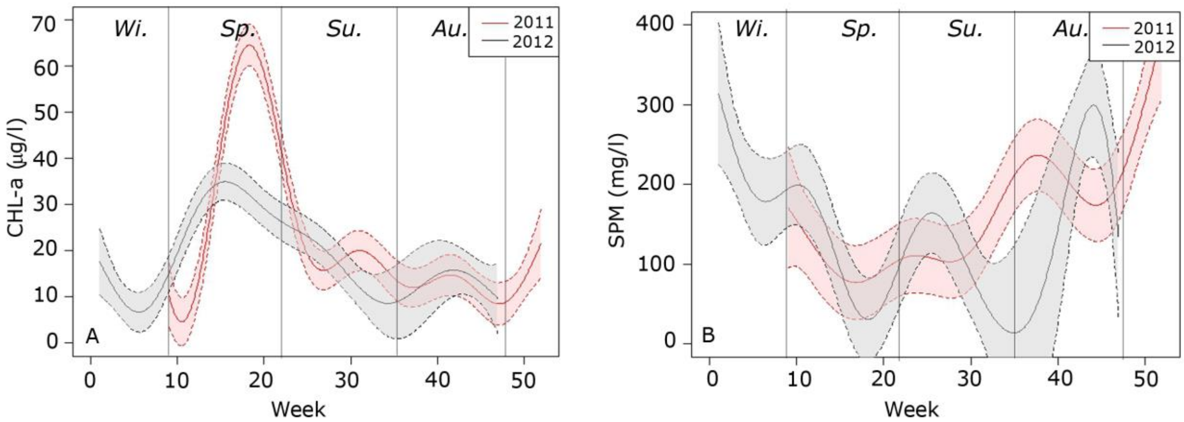

Figure 8. The GAM modeled seasonal cycles in the CHL-a (panel A) and SPM (panel B) concentrations at 0.3 mab over the period February 2011 – November 2012 on basis of weekly averaged concentrations. The shaded areas provide the 95% confidence around the estimates (Wood 2006). The seasons are indicated at the top of the graphs. In September 2012 (week 35 – 39) no (concentration) data was recorded, but estimated by the model. Therefore the confidence range is larger in this period.

3.2.4. The tidal scale

In Figure 9 the power spectral density (PSD) estimates for the SPM and CHL-a concentrations at 0.3 and 1.4 mab are shown, besides those for the current velocity and the water level. The current velocities and the water level show peaks at the lunar tidal frequencies. The focus on the M_2 and M_4 frequencies in Figure 9B reveals a contribution of the S_2 tide, though an order of magnitude smaller. The interaction of the M_2 and S_2 frequencies generates the spring-neap cycle. The PSDs of the SPM and CHL-a concentrations show also peaks corresponding to the lunar tidal frequencies. The PSD estimate of the SPM concentration at 0.3 mab has three peaks at frequencies corresponding to the tidal frequencies M_2, M_4 and M_8. At 1.4 mab similar peak frequencies, but lower and broader spectral peaks occur. In SPM and CHL-a, M_4 is particularly strong, an indication of the semi-diurnal resuspension (i.e. with each ebb and flood). The PSD of the CHL-a concentration at 0.3 mab and at 1.4 mab has four peaks at frequencies corresponding to the tidal frequencies M_2, M_4, M_6 and M_8. Compared to the SPM concentration, the CHL-a concentration oscillates at an additional frequency i.e. the M_6 tidal frequency. The largest spectral peak of the CHL-a concentration at 0.3 mab is at the

M_4 frequency, while at 1.4 mab the M_2 equals the M_4 peak. As the spectral peaks of the SPM and CHL-a concentrations are already broader than those of the velocities and water level, it is difficult to distinguish their spring-neap oscillation.

Figure 10 gives three examples of the tidal variation in the concentrations of SPM and CHL-a during two calm conditions and during a storm. The left panels are from October 2nd-3rd 2011 after a long period of calm weather. The middle panels are at the end of a storm (H_s ~ 3 - 4 m). The right panels represent October 14th-15th 2011, 2 days after a 6-day storm period. In the left and right-hand panels the bed shear stress and the wave height have a similar magnitude, but the tidal oscillation of the SPM concentration after the storm is one order of magnitude larger than before. The range of the intratidal SPM variation appeared quite large with an average of 60 mgl^{-1} before the storm and up to 400 mgl^{-1} after the storm. Notably, during the storm still a tidal signal is apparent, but less clear. During both calm periods 8 SPM concentration peaks appear at the 8 velocity peaks (4 flood and 4 ebb) corresponding to the M_4 spectral peak in the concentration and the M_2 spectral peak in the velocity. The most obvious relation of the concentration signal with the tide forms the exact correspondence in timing of the SPM and CHL-a minima and the slack tides (i.e. minimal velocities). On the other hand, the timing of the concentration peaks has a phase difference with the tidal current peaks, varying per tide, showing concentration peaks either before or after the maximum current velocity. Sometimes the concentration maxima are double-peaked.

During the calm period the CHL-a concentration oscillation with the tidal current is smaller than the SPM oscillation, with 4 CHL-a peaks barely noticeable for 8 velocity peaks (Figure 10C). During and after the storm period the CHL-a concentrations show exactly the same signal as the SPM concentrations, as if being merged together (Figure 10G). Figure 10 suggests that the contribution of CHL-a to the SPM is different before and after the storm.

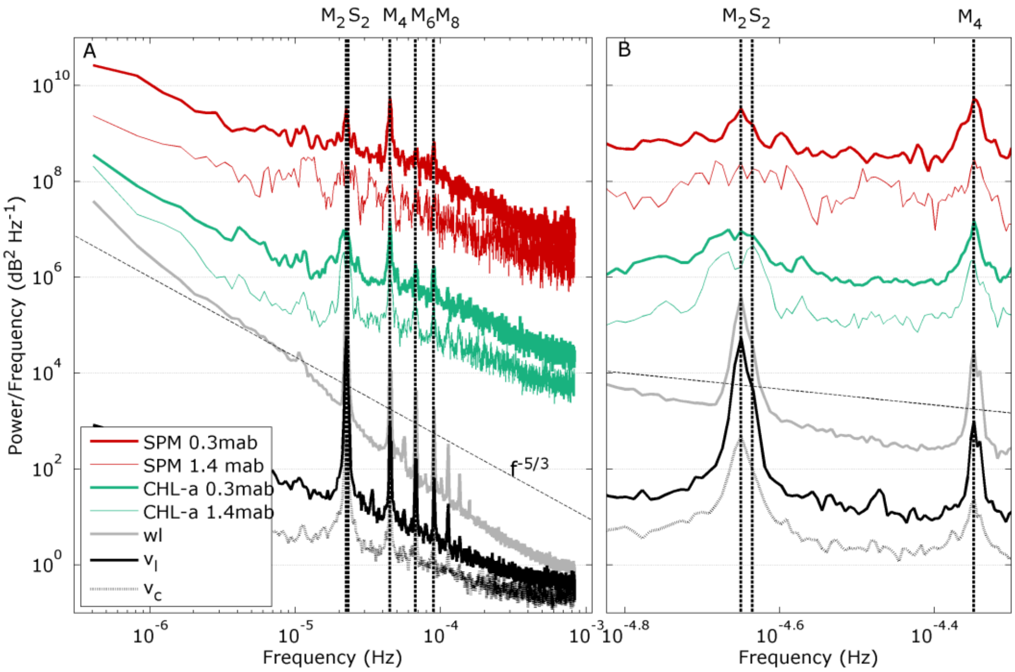

Figure 9. Power spectral density (PSD) estimates of the SPM concentrations, the CHL-a concentrations, the water level and the current velocity; both alongshore (v_l) and cross-shore (v_c). The PSDs are calculated with the Welch method with a window length of 4000 over the period March 1st 2011 – July 1st 2012. The main lunar tidal frequencies (M_2, M_4, M_6 and M_8) and S_2 are indicated by vertical dashed lines. Indicated as well is the -5/3 slope (black dashed line), which is indicative for the inertial subrange. On the right is a zoom on the M_2, S_2 and M_4 frequencies of all variables.

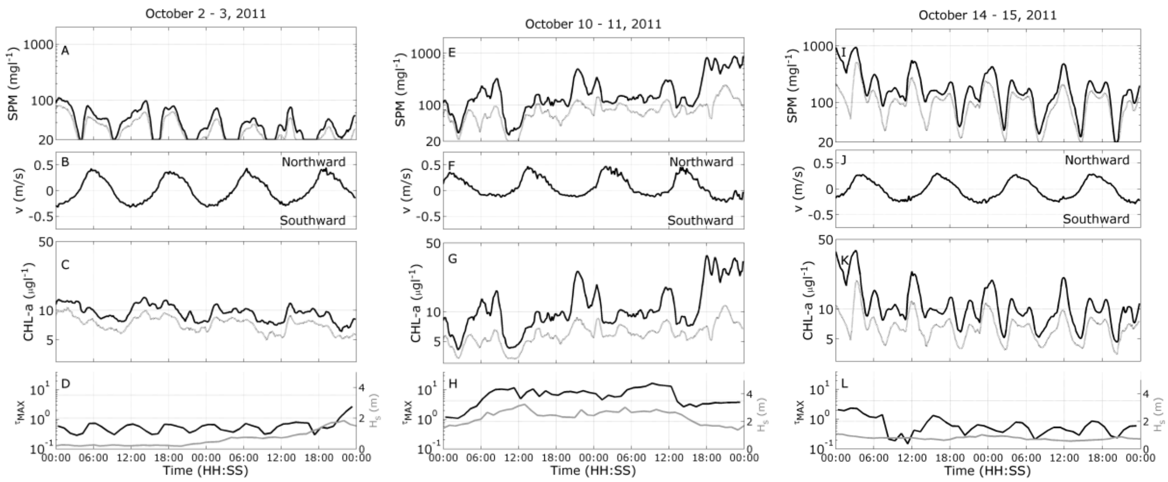

Figure 10. The variation of the SPM and the CHL-a concentrations over 48 h after a calm period (panels A-D; October 2-3, 2011), during a storm (panels E-H; October 10-11) and after a storm period (panels I-L; October 14-15, 2011). Panels A, E and I show the SPM concentrations at 0.3 mab (black)

and 1.4 mab (grey) during all periods. Panels B, F and J give the alongshore current velocities. Panels C, G and K show the CHL-a concentrations at 0.3 mab (black) and 1.4 mab (grey). Panels D, H and L give the variation of the bed shear stress (τ_{MAX}; black line; logarithmic scale) and the significant wave height (H_s; grey line; linear scale).

3.2.5. The effect of the wave climate

In Figure 11 the SPM concentration at 0.3 mab is plotted against the bed shear stress. The scatter plot shows a large spread of the data, and the tidal variation of the bed shear is visible for τ_{MAX} = 0.2 - 1 Nm^{-2}. Three observations can be drawn from the relation between bed shear stress and the near-bed SPM concentration. The first is a positive relation between the bed shear stress and the SPM concentration; i.e. increasing bed shear stresses due to waves lead to an increase in the SPM concentration. The second observation is that the median concentration has a peak at a shear stress of 6 Nm^{-2} (coinciding with median H_s = 2.5 m). And lastly, peak SPM concentrations (> 1 gl^{-1}) do not occur at maximum shear stresses but at shear stresses between 0.4 and 15 Nm^{-2}. The explanation for these last two observations is shown in the middle panel of Figure 10. Peak SPM concentrations arise in the aftermath of the storm, at 18:00 on October 11, while during the storm the SPM concentration has lower values. The decreasing shear stress initiates sinking of SPM into a high concentration suspension layer near the seabed. An analysis of the wave direction showed only a marginal effect of the wave direction on the magnitude of the SPM concentration.

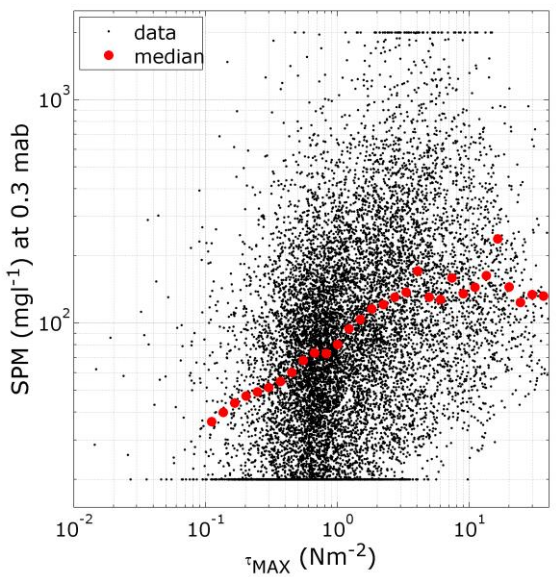

Figure 11. Scatter plot of the SPM concentration and the bed shear stress at 0.3 mab. The large red dots are the median SPM concentrations.

3.3. The vertical profile

3.3.1. Frequency distribution

The SPM and CHL-a concentrations have a skewed distribution to the left at all four heights, and therefore their frequency distributions are described by both the lognormal and the exponential distribution (Figure 12). The geometric mean and standard deviation (lognormal distribution) and rate parameter (exponential distribution) are given in Table 1. As the dataset covers one year and nine months (one winter is missing), the dataset was split in two overlapping year-long time series: March 2011 - March 2012 and July 2011 – July 2012. There was no bias found for the resulting dataset length regarding the SPM concentrations since the average and standard deviation of the 1.8 year dataset were similar to those of the two subsets. For both variables the geometric mean decreases from the seabed upward. For the SPM concentrations the decrease is logarithmically from 83 mgl^{-1} to 45 mgl^{-1}. However, the geometric mean of the CHL-a concentrations decreases only between 0.3 and 0.8 mab from 13.7 to 9.2 µgl^{-1}, and remains constant between 0.8 and 2.0 mab.

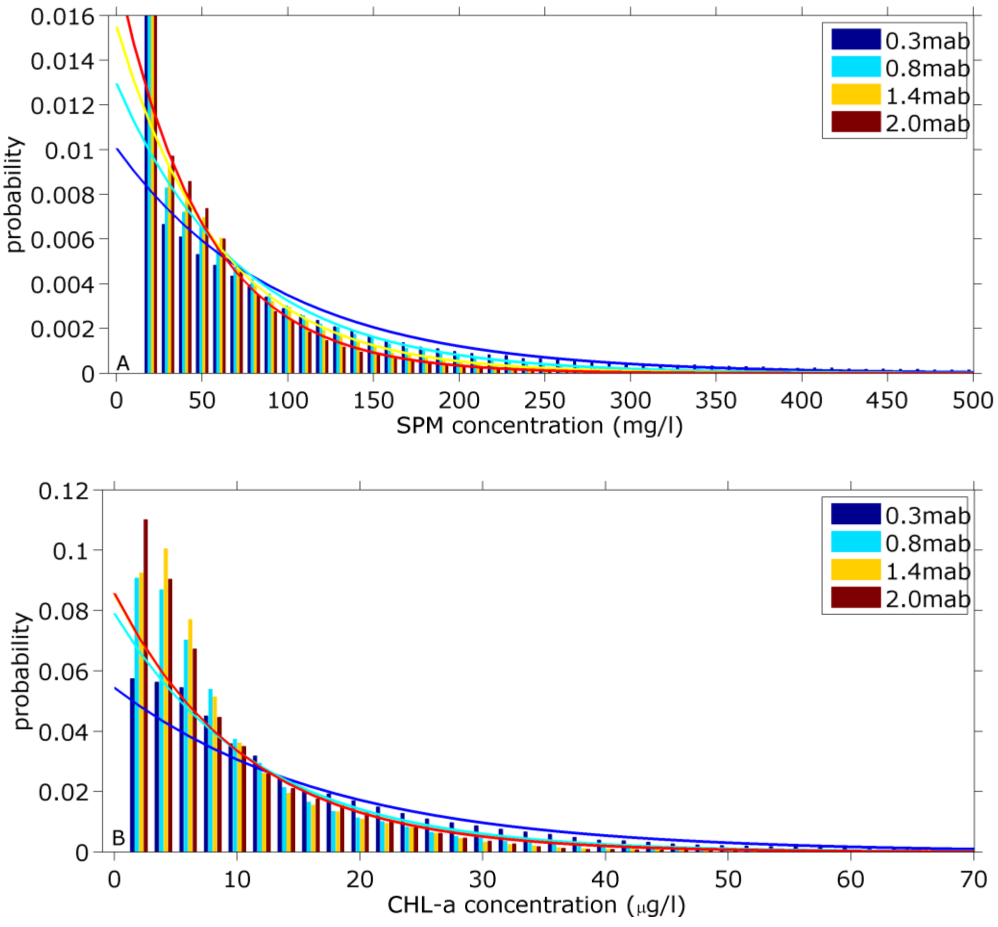

Figure 12. Frequency distributions of the SPM (A) and CHL-a (B) concentrations at 0.3 m, 0.8 m, 1.4 m, and 2.0 m above the seabed, both the histogram and the fitted exponential function.

Table 1. Calculated geometric mean and geometric standard deviation (std) and rate parameter (λ) of the exponential distribution of the SPM (in mgl^{-1}) and the CHL-a (in µgl^{-1}) concentrations at all four heights.

	SPM			CHL-a		
	geo. mean (mg l^{-1})	geo. std	λ (mg l^{-1})	geo. mean (µg l^{-1})	geo. std	λ (µg l^{-1})
2.0 mab	45	2.4	59	9.1	2.3	11
1.4 mab	49	2.6	66	8.7	2.2	11
0.8 mab	60	2.7	80	9.2	2.3	12
0.3 mab	83	3.3	106	13.7	2.4	18

3.3.2 Rouse numbers and profiles

For 84% of the profiles with SPM concentrations between 20 and 2000 mgl^{-1} the fit had an R^2 larger than 0.95 and thus followed a Rouse profile from which a reliable R_n could be calculated. About 26% of the profiles had a concentration either below 20 mgl^{-1} or above 2000 mgl^{-1} and were omitted from the analyses. These concentrations could not reliably be detected by the sensors and thus cannot give a reliable estimate of R_n. The R_n was positively correlated with the concentration at 0.3 mab (R^2 = 0.6). The CHL-a concentration profiles fitted the Rouse profile only for 2% of the data, and are therefore not included in further analyses. This result confirms the result in section 3.3.1 concerning the difference between the uniform CHL-a distribution upward of 0.8 mab and the logarithmic SPM distribution.

The calculated Rouse number for the SPM profiles varied over time both at the tidal and the episodic storm scale between 0.01 and 2.5 (Figures 4I and 5I) which suggests a wide variety of SPM concentration profiles. By extrapolating the near-bed measurements up to the surface following the Rouse profile, the SPM profiles can be divided into a near-bed suspension (R_n > 0.8) and a mixed suspension (R_n < 0.8) (Mehta, 2014). In 90 % of the time R_n is found to be smaller than 0.8, and thus the SPM is dominantly present in a mixed suspension, *ie.* the SPM profile is more uniform up to the water surface. In a small percentage of the time (10%) the SPM suspension is concentrated in the near-bed layer (near-bed suspension).

The temporal variation in the percentage of SPM profiles following a rouse profile (R^2 > 0.95) is also shown in Figures 4I and 5I and quantified as the parameter Q_p, which is the percentage of well-fitted Rouse profiles per tidal cycle. The average value of Q_p is 88%, with low Q_p predominantly apparent in March 2011, and February / March 2012. It appeared that SPM profiles with a reference concentration (at z_a = 0.3 mab) larger than 500 mgl^{-1} always followed a Rouse profile.

To explore whether the fit of the Rouse profile to the SPM profile depended on the tidal phase, the percentage of accepted and rejected Rouse profiles is plotted against the alongshore current velocity (Figure 13). This figure is based on the tides with less than 20% rejected Rouse profiles (Q_p > 80%) to eliminate causes of potential deviations other than the tidal flow. From the figure it is evident that during all phases of the tidal cycle Rouse profiles are rejected (blue bars in Figure 13B). The highest percentage of rejected Rouse profiles is found at low current velocities and more precisely at the accelerating flow after slack tide up to 0.5 of the maximum tidal velocity (Figure 13A).

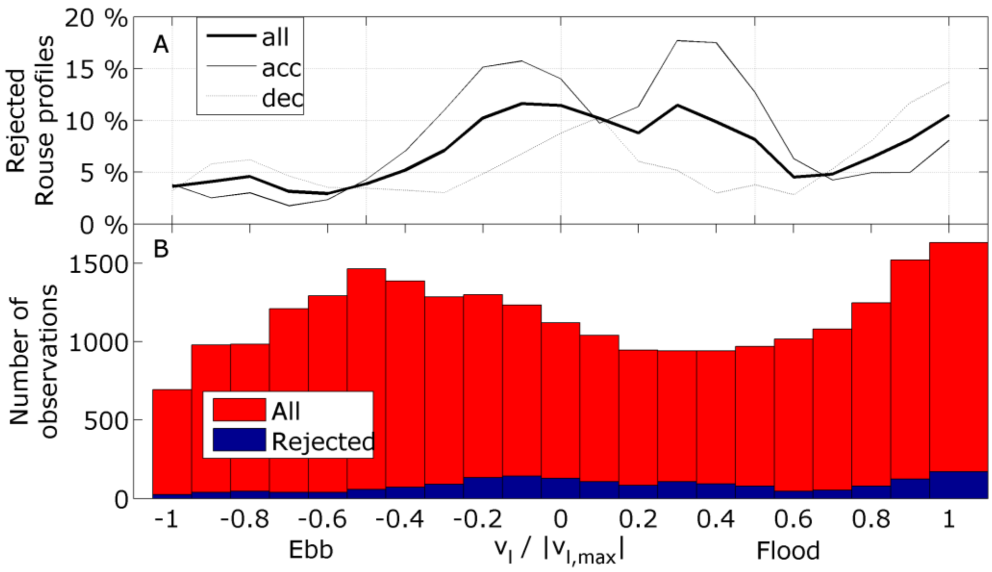

Figure 13. A: Percentage of rejected Rouse profiles per phase of the tide. The latter is calculated as the alongshore velocity divided by the maximum alongshore velocity of the tidal cycle. The graph shows the percentage rejected of all tides with Q_p *> 80%, and the percentages when the velocities are separated in accelerating (acc) and decelerating (dec) tidal currents. B: The raw numbers of the rejected observations and all selected observations per tidal phase.*

4. Discussion

4.1. Seasonality

The long-term signals of the near-bed SPM and CHL-a concentrations show opposite seasonal cycles in the Dutch coastal zone (Figure 8). A seasonal cycle in the SPM concentrations (high in winter, low in summer) has also been reported for similar environments, such as the Irish Sea (Jago et al., 2007) and other parts of the southern North Sea (Blauw et al., 2012; Fettweis et al., 2012). In these studies the wave climate was the main driver of the seasonal SPM variation (Stanev et al., 2009). Our study confirms this larger role of the wave climate, since the bed shear stress – the principal parameter for SPM resuspension – is logarithmically related to the wave height and reaches values up to two orders of magnitude larger for wave heights than the tidal current (Figure 7).

Recently however, Fettweis et al. (2014) suggested that the seasonal variation in SPM is primarily governed by the seasonal variation in organic matter, and suggested the wave climate as a secondary process. They presented a seasonal variation in the floc aggregation due to the variation in organic matter, hence in fall velocity, leading to a seasonal signal in the settlement of SPM. It is indeed conceivable that after the initial decrease of SPM concentrations, the first phytoplankton bloom initiates a possible feedback loop, in which the freshly formed organic matter facilitates SPM settlement, thereby improving light conditions even more and so on, as suggested by Blauw et al. (2012). Our summer SPM concentrations give a hint of the interference of organic matter, as in both years the summer SPM concentrations were lower than in winter for similar wave heights. Not only scavenging by sinking aggregates (Blauw et al., 2012; Jago et al., 2007; Fettweis et al., 2014), but also stabilization of fines in the seabed by the dominant *Ensis Directus* may have reduced the resuspension signal in summer (Borsje et al., 2008; Witbaard et al., 2016; this volume).

The CHL-a signal in our study shows an increase in spring - when SPM decreases-, but our results cannot point to a leading role for CHL-a in the seasonal pattern of SPM. A translation from CHL-a concentrations to phytoplankton species, to excretion of (sticky) polysaccharides, to aggregate floc sizes and finally SPM settlement cannot be made. Also, we do not know if and how the spring increase in the near-bed accumulated CHL-a signal is representative of the phytoplankton growth higher up in the water column, or to what extent a phase lag exists at this shallow site. Our results do point to a principal role for the wave climate in the seasonal variation of SPM. The oscillations in the seasonal SPM concentration show a good agreement with the different variations in the wave climate in both years.

4.2 Fluffy layer development

Waves increased the tidal bed shear stress range of 0.2 - 1 Nm^{-2} with one to two orders of magnitude up to 40 Nm^{-2} (Figure 7). These high bed shear stresses mobilize the seabed and resuspend large amounts of sediment. Remarkably, the maximum SPM concentrations exceeding 1 gl^{-1} were not measured at the peak of the storms (Figure 11), but arose in the aftermath (Figure 10E). The relative low concentrations during the heaviest storms may have two reasons. Firstly, they may have been caused by the low sensor sensitivity for sand grains. Optical backscatter is known to be sensitive for the finest particles and thus not fully representative for the resuspension of the grain size range of the seabed (Connor and De Visser, 1992). Another likely explanation is however the unbalance between the release rate of fines during the development of a storm and the high sinking rates in the aftermath of a storm.

Over the course of a storm development (buried) fines are gradually resuspended from deeper sediment layers and are thus slowly released. At increasing bed shear stresses fines from deeper and deeper layers are "washed out" and mixed over the entire water column where it forms a diluted suspension. Once the storm has passed and wave action decreases, the sediment load from the entire water column starts to settle and accumulates in a confined layer near the seabed: an increase in SPM concentration at 0.3 mab at low turbulence levels (Figure 10E). The high Rouse numbers for high concentrations (linear relation R_n with C_a) indicate a steep vertical concentration gradient, which supports the development of a highly concentrated fluffy layer close to the seabed after a storm.

This (fluffy) layer also contains high concentrations of CHL-a rich particles that settle to the seabed over time. The settlement, subsequent burial and following resuspension of CHL-a concentrations is not uncommon and has been observed before (Boon and Duineveld, 1998; Jago et al., 2007). Such settlement leads to higher levels of near-bed CHL-a concentrations than surface water concentrations (order of 10 μgl^{-1} (Joordens et al., 2001)). The high abundance of CHL-a in the study area close to the seabed is a possible explanation for the high abundance of the benthic filter feeder *Ensis directus* in the area (Witbaard et al., 2015).

4.3 Tidal scale resuspension

The spectral analysis (Figure 9) and the 48 hour zooms (Figure 10) indicated that SPM and CHL-a concentrations have a tidal oscillation. Single point observations always make it difficult to assess whether SPM variations are caused by local resuspension and settling processes or by horizontal advection, as both processes create similar concentration signals (Bass et al., 2002; Blewett and Huntley, 1999; Jago et al., 2006). In our study area both processes may act, as the requirements for both are present: 1) a horizontal gradient in the SPM concentration (Figure 1) and 2) a local source (fluffy layer above the sandy seabed).

The spectral analysis (Figure 9) identified M_4 as the main tidal component in both the SPM and the CHL-a dataset, followed by the M_2 component. The spring-neap cycle could not be distinguished in the signal due to the flattening of the spectral peaks: a result of the phase differences of the peak concentrations with respect to the velocity peaks. The presence of the M_4 signal can be due to both the resuspension and settling process and the advection of a concentration gradient back and forth along the bottom frame with the M_2 tide (Blewett and Huntley, 1998). The advective component may be detected as a phase difference between the peaks of the concentration and the velocity, whereas the resuspension process has no phase differences - when measured close the seabed (Bass et al., 2002). As the troughs in the SPM concentration time-series coincided clearly with the slack periods of the tidal cycle, we suggest resuspension takes up a larger role than advection.

The M_2 component in the concentration signals may have multiple causes, amongst others a difference in resuspension strength by the ebb (weaker) and flood (stronger) currents, but also the sensitivity of the optical sensor to the aggregation and break-up process on the tidal cycle has been observed (Jago et al., 2006). The latter produces a typical ‘twin-peak signature’ in the concentration time-series of which a modified version can be observed in Figure 10 before and after the storm.

4.4 Cross-shore advection

Advective transport can occur both in the alongshore and the cross-shore direction. In both directions the velocity spectra displayed M_2 as the principal tidal component (Figure 9). In the alongshore direction the velocities are largest (Figures 4E and 5E) but the concentration gradient is small and not accurately known (Van der Hout et al., 2015). In the cross-shore direction the velocities are small but the concentration gradient is large (Figure 1). Two processes can generate a cross-shore oscillation on the tidal scale; the tidal ellipse (a continuous process; Houwman, 2000) and tidal straining (an infrequent process; Simpson et al., 1993). As the discrimination between both processes is a study in itself, we will here only focus on the measured quantities.

The question is how much the cross-shore advection may contribute to the tidal SPM concentration variation measured at the bottom frame: on average 84 mgl^{-1} at 1.4 mab and 174 mgl^{-1} at 0.3 mab. By combining SPM concentration data obtained from the spatial observations in 2010-2011 (Van der Hout et al., 2015) with time series obtained from the bottom frame, we can estimate the range of the SPM concentration variation resulting from the cross-shore oscillation. From the ship-based observations (van der Hout et al., 2015) a cross-shore SPM concentration gradient 0.035 ± 0.015 mgl^{-1} per meter at 1.2 mab is estimated (Figure 14). The trend of the vertical profiles in Figure 14 suggests that the near-bed cross-shore gradient at 0.3 mab may be even stronger. To estimate the cross-shore tidal water displacement a harmonic analysis was performed on the velocity data from the bottom frame, followed by a primary and secondary axis decomposition of the M_2 component. The average amplitude of the minor axis appeared 0.02 ms^{-1}, the maximum is 0.09 ms^{-1}. The resulting cross-shore tidal water displacement is 280 m for the average amplitude and 1300 m for the maximum amplitude. Multiplied by the average cross-shore SPM concentration gradient, the average magnitude of the tidal SPM concentration variation at 1.2 mab due to cross-shore advection would be 9.8 mgl^{-1}, and the maximum 65 mgl^{-1}. Thus the cross-shore advection may contribute substantially to the variation in SPM concentrations when compared to the median tidal variation of 84 mgl^{-1} at 1.4 mab but is on average only 12%. This enforces our previous suggestion that on the tidal scale resuspension is dominant over advection. Summarizing, with the alternating tidal current the space-varying SPM field is moving up and down (resuspension - settling) while moving back and forth (advection) along the study site and possibly changing the aggregation form of the flocs.

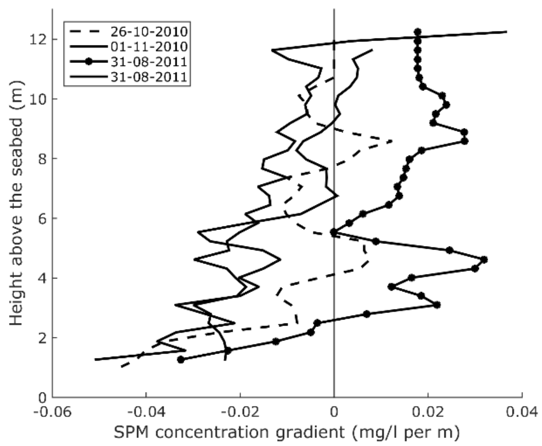

Figure 14. The vertical profiles of the horizontal SPM concentration gradient at the frame location. No data closer to the seabed is available than 1.2 mab. The SPM concentrations were measured during four surveys along the Egmond transect in 2010 and 2011 (Van der Hout et al., 2015), the dates of the visit are indicated in the legend. Positive SPM concentration gradients indicate

an increase in concentration towards the shore; negative values indicate a decrease in SPM concentrations towards the shore.

4.5. Rouse profiles

A logarithmic Rouse profile fitted to 84% of the SPM profiles, but not to the CHL-a profiles. The disparity in the quality of the fits of the CHL-a and SPM profiles suggests that although CHL-a is aggregated in flocs of SPM, the aggregation is not uniform in the near-bed layer. A dependence of R_n on C_a is observed at our study site, similar to other studies (Orton and Kineke, 2001), which is a violation of one assumptions for the Rouse profile. Apparently this underlying assumption is not a strict requirement. Care should be taking with applying the Rouse profile at low SPM concentrations and more specifically near slack tides, where most poorly-fitting profiles were found. Whereas Orton and Kineke (2001) excluded a small period around slack (range of 0.01 ms^{-1}) from their analysis, we found that rejection occurred predominantly at the accelerating current after slack and up to a velocity of 50 % of the maximum current. The sensitivity of the profile fit at low concentrations is possibly due to the slow response of the low concentration particles to quickly changing conditions (Orton and Kineke, 2001).

The calculated Rouse numbers showed that in 90 % of the time the SPM profile is a mixed suspension, suggesting that SPM concentrations at the surface are in the same order of magnitude as the near-bed concentrations. This implies that both the near-bed layer and the surface layer should be taken into account when considering transport estimates of SPM in further research. The contribution of the 10% bed load transport to the total transport should not be underestimated, as these profiles with a high R_n also have the highest SPM concentrations (R_n ~ C_a). Although 84% of the SPM concentrations profiles could be fitted to the Rouse profile, extrapolating the near-bed data up to the surface with the Rouse method should be done with care in this study area as the observed periodic vertical stratification (Rijnsburger et al., 2016; Van der Hout et al., 2015) may temporarily inhibit SPM resuspension up to the surface (Jones et al., 1998; Joordens et al., 2001).

5. Conclusion

From the analysis and discussion of the various variables and time scales we can summarize that in the TMZ a fluffy layer exists close to the seabed which consists of accumulated SPM and CHL-a rich material. The SPM consists mainly of fine silt with a high organic content, and appears dominantly in aggregated form. For significant wave heights larger than 0.8 m the resuspension by waves dominates the near-bed SPM and CHL-a concentration variation over the tidal resuspension. During storms the seabed can become depleted, after which the high concentrated fluffy layer forms again by the settlement of the temporarily redistributed particles. On the regular tidal scale a part of the SPM and CHL-a remains in the resuspension - settling mode, and is at the same time advected back and forth in both the alongshore and cross-shore direction. The seasonal CHL-a concentration is dominated by the spring bloom, but shows also resuspension by waves. The seasonal SPM concentration is primarily driven by the seasonal wave climate; high in autumn and winter, low in spring and summer. A secondary actor forms the seasonal activity of organic matter and biota, which have an opposing seasonal cycle to the SPM.

Acknowledgements

This work has been made possible by the financial support (ref no. LM-006588) of a collaboration between the La Mer Foundation and the Ministry of Infrastructure and Environment (Rijkswaterstaat, The Netherlands) and of a grant of Ecoshape (project no. NTW3.1) within the framework of Building with Nature. The practical work could not have been done without the enormous input of the crews of MS *Terschelling* and RV *Pelagia* and colleagues on board. We would like to thank Felix Temmesfeld and Jan-Berend Stuut for the processing and the analysis respectively of the grain size samples. Leo Maas and Hans van Haren are gratefully acknowledged for their advice on the turbulence data, and Maarten Kleinhans on the wave friction factor. Piet Hoekstra and two anonymous reviewers are acknowledged for their critical advice on the first manuscript. We thank the Ministry of Infrastructure and Environment (Rijkswaterstaat, The Netherlands) for the wave data and the Royal Netherlands Meteorological Institute (KNMI, The Netherlands) for the wind data.

References

Bass, S.J., Aldridge, J.N., McCave, I.N., Vincent, C.E., 2002. Phase relationships between fine sediment suspensions and tidal currents in coastal seas. J. Geophys. Res. 107, 3146. doi:10.1029/2001JC001269

Blauw, A.N., Benincà, E., Laane, R.W.P.M., Greenwood, N., Huisman, J., 2012. Dancing with the tides: fluctuations of coastal phytoplankton orchestrated by different oscillatory modes of the tidal cycle. PLoS One 7, e49319. doi:10.1371/journal.pone.0049319

Blewett, J., Huntley, D., 1999. Measurement of Suspended Sediment Transport Processes in Shallow Water off the Holderness Coast, UK. Mar. Pollut. Bull. 37, 134–143. doi:10.1016/S0025-326X(99)00092-2

Boon, A., Duineveld, G., 1998. Chlorophyll a as a marker for bioturbation and carbon flux in southern and central North Sea sediments. Mar. Ecol. Prog. Ser. 162, 33–43. doi:10.3354/meps162033

Borsje, B.W., van Wesenbeeck, B.K., Dekker, F., Paalvast, P., Bouma, T.J., van Katwijk, M.M., de Vries, M.B., 2011. How ecological engineering can serve in coastal protection. Ecol. Eng. 37, 113–122. doi:10.1016/j.ecoleng.2010.11.027

Conner, C.S., De Visser, A.M., 1992. A laboratory investigation of particle size effects on an optical backscatterance sensor. Mar. Geol. 108, 151–159. doi:10.1016/0025-3227(92)90169-I

De Jong, M.F., Baptist, M.J., Lindeboom, H.J., Hoekstra, P., 2015. Short-term impact of deep sand extraction and ecosystem-based landscaping on macrozoobenthos and sediment characteristics. Mar. Pollut. Bull. 97, 294 – 308.

Dyer, K.R., Moffatt, T.J., 1998. Fluxes of suspended matter in the East Anglian plume Southern North Sea. Cont. Shelf Res. 18, 1311–1331.

Eleveld, M.A., Pasterkamp, R., van Der Woerd, H.J., Pietrzak, J.D., 2008. Remotely sensed seasonality in the spatial distribution of sea-surface suspended particulate matter in the southern North Sea. Estuar. Coast. Shelf Sci. 80, 103–113. doi:10.1016/j.ecss.2008.07.015

Fettweis, M., Baeye, M., Van der Zande, D., Van den Eynde, D., Lee, B.J., 2014. Seasonality of floc strength in the southern North Sea. J. Geophys. Res. Ocean. 119, 1911–1926. doi:10.1002/2013JC009750

Fettweis, M., Monbaliu, J., Baeye, M., Nechad, B., Van den Eynde, D., 2012. Weather and climate induced spatial variability of surface suspended particulate matter concentration in the North Sea and the English Channel. Methods Oceanogr. 3-4, 25–39. doi:10.1016/j.mio.2012.11.001

Fettweis, M., Nechad, B., Van Den Eynde, D., 2007. An estimate of the suspended particulate matter (SPM) transport in the southern North Sea using SeaWiFS images, in situ measurements and numerical model results. Cont. Shelf Res. 27, 1568–1583. doi:10.1016/j.csr.2007.01.017

Goring, D.G., Nikora, V.I., 2002. Despiking Acoustic Doppler Velocimeter Data. J. Hydraul. Eng. 128, 117–126.

Houwman, K., 2000. Tide, wind- and wave-driven flow processes in the nearshore zone. PhD Thesis. Utrecht University.

Howarth, M.J., Simpson, J.H., Sündermann, J., van Haren, H., 2002. Processes of Vertical Exchange in Shelf Seas (PROVESS). J. Sea Res. 47, 199–208.

Huthnance, J.M., 1997. The PROFILE project: an overview. J. Mar. Syst. 12, 249–261. doi:10.1016/S0924-7963(96)00101-7

Jago, C.F., Jones, S.E., Sykes, P., Rippeth, T., 2006. Temporal variation of suspended particulate matter and turbulence in a high energy, tide-stirred, coastal sea: Relative contributions of resuspension and disaggregation. Cont. Shelf Res. 26, 2019–2028. doi:10.1016/j.csr.2006.07.009

Jago, C.F., Kennaway, G.M., Novarino, G., Jones, S.E., 2007. Size and settling velocity of suspended flocs during a Phaeocystis bloom in the tidally stirred Irish Sea, NW European shelf. Mar. Ecol. Prog. Ser. 345, 51–62. doi:10.3354/meps07006

Jones, S.E., Jago, C.F., Bale, a. J., Chapman, D., Howland, R.J.M., Jackson, J., 1998. Aggregation and resuspension of suspended particulate matter at a seasonally stratified site in the southern North Sea: physical and biological controls. Cont. Shelf Res. 18, 1283–1309. doi:10.1016/S0278-4343(98)00044-2

Joordens, J.C.A., Souza, A.J., Visser, A., 2001. The influence of tidal straining and wind on suspended matter and phytoplankton distribution in the Rhine outflow region. Cont. Shelf Res. 21, 301–325. doi:10.1016/S0278-4343(00)00095-9

Krivtsov, V., Gascoigne, J., Jones, S.E., 2008. Harmonic analysis of suspended particulate matter in the Menai Strait (UK). Ecol. Modell. 212, 53–67. doi:10.1016/j.ecolmodel.2007.10.039

McCandliss, R.R., Jones, S.E., Hearn, M., Latter, R., Jago, C.F., 2002. Dynamics of suspended particles in coastal waters (southern North Sea) during a spring bloom. J. Sea Res. 47, 285–302. doi:10.1016/S1385-1101(02)00123-5

Mehta, A.J., 2014. An Introduction to Hydraulics of Fine Sediment Transport. World Scientific Publishing Co. Pte. Ltd., Singapore.

Mori, N., Suzuki, T., Kakuno, S., 2007. Noise of Acoustic Doppler Velocimeter Data in Bubbly Flows. J. Eng. Mech. 133, 122–125.

Nauw, J.J., van der Vegt, M., 2012. Hydrodynamics of the Rhine ROFI near IJmuiden. NCK-days 2012 Crossing borders Coast. Res. Jubil. Conf. Proc. 1. doi:10.3990/2.191

Orton, P.M., Kineke, G.C., 2001. Comparing Calculated and Observed Vertical Suspended-Sediment Distributions from a Hudson River Estuary Turbidity Maximum. Estuar. Coast. Shelf Sci. 52, 401–410. doi:10.1006/ecss.2000.0747

Passow, U., 2002. Transparent exopolymer particles (TEP) in aquatic environments. Prog. Oceanogr. 55, 287–333. doi:10.1016/S0079-6611(02)00138-6

Rijnsburger, S., van der Hout, C.M., van Tongeren, O., de Boer, G.J., van Prooijen, B.C., Borst, W.G., Pietrzak, J.D., 2016. Simultaneous measurements of tidal straining and advection at two parallel transects far downstream in the Rhine ROFI. Ocean Dyn. 66, 719–736. doi:10.1007/s10236-016-0947-x

Roberts, J.F., Champion, a. J., Dawkins, L.C., Hodges, K.I., Shaffrey, L.C., Stephenson, D.B., Stringer, M. a., Thornton, H.E., Youngman, B.D., 2014. The XWS open access catalogue of extreme European windstorms from 1979–2012. Nat. Hazards Earth Syst. Sci. Discuss. 2, 2011–2048. doi:10.5194/nhessd-2-2011-2014

Rouse, H., 1950. Engineering Hydraulics. John Wiley & Sons, Inc., New York.

Simpson, J.H., Bos, W.G., Schirmer, F., Souza, A.J., Rippeth, T.P., Jones, S.E., Hydes, D., 1993. Periodic stratification in the Rhine ROFI in the North Sea. Oceanol. Acta 16, 23–32.

Soulsby, R.L., Humphery, J.D., 1990. Field Observations of Wave-Current Interaction at the Sea Bed, in: Tørum, A., Gudmestad, O.T. (Eds.), Water Wave Kinematics. Kluwer Academic Publisher, pp. 413–428. doi:10.1007/978-94-009-0531-3_25

Stanev, E.V., Dobrynin, M., Pleskachevsky, A., Grayek, S., Günther, H., 2009. Bed shear stress in the southern North Sea as an important driver for suspended sediment dynamics. Ocean Dyn. 59, 183–194. doi:10.1007/s10236-008-0171-4

Stuut, J.B.W., Prins, M.A., Fred Jansen, J.H., 2002. Fast reconnaissance of carbonate dissolution based on the size distribution of calcareous ooze on Walvis Ridge, SE Atlantic Ocean. Mar. Geol. 190, 581–589. doi:10.1016/S0025-3227(02)00478-4

Stuut, J.B.W., Temmesfeld, F., De Deckker, P., 2014. A 550ka record of aeolian activity near north west cape, Australia: Inferences from grain-size distributions and bulk chemistry of SE Indian ocean deep-sea sediments. Quat. Sci. Rev. 83, 83–94. doi:10.1016/j.quascirev.2013.11.003

Van Alphen, J.S.L.J., 1990. A mud balance for Belgian-Dutch coastal waters between 1969 and 1986. Netherlands J. Sea Res. 25, 19–30.

Van der Giessen, A., de Ruijter, W.P.M., Borst, J.C., 1990. Three-dimensional current structure in the Dutch coastal zone. Netherlands J. Sea Res. 25, 45–55.

Van der Hout, C.M., Gerkema, T., Nauw, J.J., Ridderinkhof, H., 2015. Observations of a narrow zone of high suspended particulate matter (SPM) concentrations along the Dutch coast. Cont. Shelf Res. 95, 27–38. doi:10.1016/j.csr.2015.01.002

Van der Veer, H.W., Dapper, R., Henderson, P.A., Jung, A.S., Philippart, C.J.M., Witte, J.I., Zuur, A.F., 2015. Changes over 50 years in fish fauna of a temperate coastal sea: Degradation of trophic structure and nursery function. Estuar. Coast. Shelf Sci. 155, 156–166.

Van Raaphorst, W., Phillippart, C.J.M., Smit, J.P.C., Dijkstra, F.J., Malschaert, J.F.P., 1998. Distribution of suspended particulate matter in the North Sea as inferred from NOAA/AVHRR reflectance images and in situ observations. J. Sea Res. 39, 197–215. doi:10.1016/S1385-1101(98)00006-9

Van Rijn, L.C., 2007. Unified View of Sediment Transport by Currents and Waves. I: Initiation of Motion, Bed Roughness, and Bed-Load Transport. J. Hydraul. Eng. 133. doi:dx.doi.org/10.1061/(ASCE)0733-9429(2007)133:6(649)

Verney, R., Deloffre, J., Brun-Cottan, J.C., Lafite, R., 2007. The effect of wave-induced turbulence on intertidal mudflats: Impact of boat traffic and wind. Cont. Shelf Res. 27, 594–612. doi:10.1016/j.csr.2006.10.005

Visser, M., de Ruijter, W.P.M., Postma, L., 1991. The distribution of suspended matter in the Dutch coastal zone. Netherlands J. Sea Res. 27, 127–143.

Wiberg, P.L., Sherwood, C.R., 2008. Calculating wave-generated bottom orbital velocities from surface-wave parameters. Comput. Geosci. 34, 1243–1262. doi:10.1016/j.cageo.2008.02.010

Witbaard, R., Bergman, M.J.N., Weerlee, E. Van, Duineveld, G.C.A., 2016. An estimation of the effects of Ensis directus on the transport and burial of silt in the near-shore Dutch coastal zone of the North Sea.

Witbaard, R., Duineveld, G.C.A., Bergman, M.J.N., Witte, H.I., Groot, L., Rozemeijer, M.J.C., 2015. The growth and dynamics of Ensis directus in the near-shore Dutch coastal zone of the North Sea. J. Sea Res. 95, 95–105.

Wood, S.N., 2006. Generalized Additive Models: An Introduction with R. Chapman and Hall/CRC.